Neutrinoless Double Beta Decay and Nuclear Matrix Elements

P. K. Raina

Department of Physics
Indian Institute of Technology Ropar, INDIA

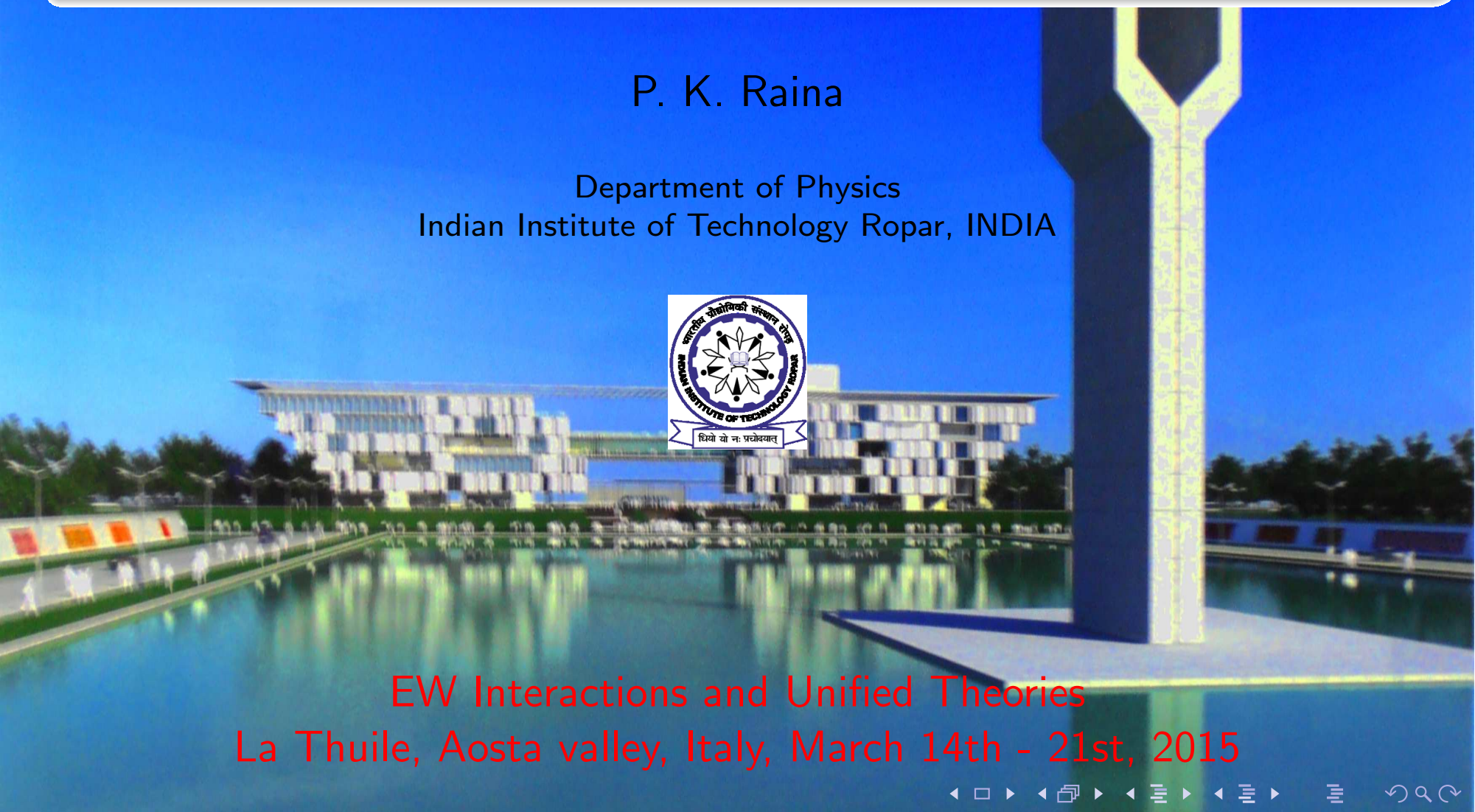

EW Interactions and Unified Theories
La Thuile, Aosta valley, Italy, March 14th - 21st, 2015

Overview

Table of Contents

Introduction & Motivation

Confirmation of neutrino flavor oscillations at atmospheric, solar, reactor, and accelerator neutrino sources SUPPLEMENTED with the possible observation of neutrinoless double beta ($0\nu\beta\beta$) decay have together played an extremely inspirational role in the advancement of a vast amount of experimental as well as theoretical studies on nuclear double-beta ($\beta\beta$) decay.

Introduction & Motivation

Confirmation of neutrino flavor oscillations at atmospheric, solar, reactor, and accelerator neutrino sources SUPPLEMENTED with the possible observation of neutrinoless double beta ($0\nu\beta\beta$) decay have together played an extremely inspirational role in the advancement of a vast amount of experimental as well as theoretical studies on nuclear double-beta ($\beta\beta$) decay.

The former has provided information on the neutrino mass square differences Δm^2_{12} and Δm^2_{31}, mixing angles θ_{12}, θ_{23} and θ_{13} and possible hierarchies in the neutrino mass spectrum.

Introduction & Motivation

Confirmation of neutrino flavor oscillations at atmospheric, solar, reactor, and accelerator neutrino sources SUPPLEMENTED with the possible observation of neutrinoless double beta ($0\nu\beta\beta$) decay have together played an extremely inspirational role in the advancement of a vast amount of experimental as well as theoretical studies on nuclear double-beta ($\beta\beta$) decay.

The former has provided information on the neutrino mass square differences Δm^2_{12} and Δm^2_{31}, mixing angles θ_{12}, θ_{23} and θ_{13} and possible hierarchies in the neutrino mass spectrum.

In addition to being the only experiment at present to test the Majorana nature of neutrinos, the latter also ascertains the role of various mechanism in different gauge theoretical models. Further, $0\nu\beta\beta$ decay is also the only experiment that has a potential to explore the maximum effective neutrino mass sensitivity to the orders of meVs.

Introduction & Motivation

Number of projects for observing the $0\nu\beta^-\beta^-$ decay

^{76}Ge (GERDA, MAJORANA), ^{82}Se (SuperNEMO, Lucifer), ^{130}Te (CUORE, SNO+), ^{100}Mo (MOON, AMoRE), ^{116}Cd (COBRA), ^{136}Xe (XMASS, EXO, KAMLand-Zen, NEXT), ^{48}Ca (CANDLES), ^{150}Nd (SuperNEMO, DCBA/ MTD) have been designed and hopefully, the reported observation of 0 $\nu\beta^-\beta^-$ decay would be confirmed in the near future.

Introduction & Motivation

Number of projects for observing the $0\nu\beta^-\beta^-$ decay

^{76}Ge (GERDA, MAJORANA), ^{82}Se (SuperNEMO, Lucifer), ^{130}Te (CUORE, SNO+), ^{100}Mo (MOON, AMoRE), ^{116}Cd (COBRA), ^{136}Xe (XMASS, EXO, KAMLand-Zen, NEXT), ^{48}Ca (CANDLES), ^{150}Nd (SuperNEMO, DCBA/ MTD) have been designed and hopefully, the reported observation of 0 $\nu\beta^-\beta^-$ decay would be confirmed in the near future.

In the short base line experiments, the indication of $\bar{\nu}_\mu \longrightarrow \bar{\nu}_e$ conversion was explained with 0.2 eV $< \Delta m^2 <$ 2 eV and $10^{-3} < \sin^2(2\theta) < 4 \times 10^{-2}$. New results of the reactor fluxes flavor short base line oscillation. The confirmation of all these observations would imply the existence of more than three massive neutrinos

Mechanisms

In the left-right symmetric model, the three possible mechanisms of $0\nu\beta^-\beta^-$ decay are the exchange of left handed light as well as heavy Majorana neutrinos and the exchange of right handed heavy Majorana neutrinos.

Mechanisms

In the left-right symmetric model, the three possible mechanisms of $0\nu\beta^-\beta^-$ decay are the exchange of left handed light as well as heavy Majorana neutrinos and the exchange of right handed heavy Majorana neutrinos.

Alternatively, the occurrence of lepton number violating Majoron accompanied $0\nu\beta\beta$ decay is also a possibility. Based on the recent experimental evidences, regarding the observability of all nine Majoron models, it has been concluded that the study of classical Majoron models is the most preferred one.

Mechanisms

In the left-right symmetric model, the three possible mechanisms of $0\nu\beta^-\beta^-$ decay are the exchange of left handed light as well as heavy Majorana neutrinos and the exchange of right handed heavy Majorana neutrinos.

Alternatively, the occurrence of lepton number violating Majoron accompanied $0\nu\beta\beta$ decay is also a possibility. Based on the recent experimental evidences, regarding the observability of all nine Majoron models, it has been concluded that the study of classical Majoron models is the most preferred one.

Bamert, Burgess, and Mohapatra 1995 NPB, it was shown that the mixing of a light sterile neutrino (mass $\ll 1$ eV) with a much heavier sterile neutrino (mass $\gg 1$ GeV) would result in observable signals in current $\beta\beta$ decay experiments, as is the case in other interesting alternative scenarios.

Mechanisms

The study of $0\nu\beta^-\beta^-$ decay within mechanisms involving light Majorana neutrinos, classical Majorons and sterile neutrinos can be performed under a common theoretical formalism.

Mechanisms

The study of $0\nu\beta^-\beta^-$ decay within mechanisms involving light Majorana neutrinos, classical Majorons and sterile neutrinos can be performed under a common theoretical formalism.

In the mass mechanism, the contributions of the pseudoscalar and weak magnetism terms of the recoil current can change the nuclear transition matrix elements (NTMEs) M(0ν) up to 30% in the QRPA, about 20% in the interacting shell model (ISM) and 15% in the interacting boson model (IBM).

Many Body Approaches and Some Inferences

In the evaluation of NTMEs, the most desirable approach is to employ the successful large scale shell-model calculations, if feasible. However, the quasiparticle random phase approximation (QRPA) and its extensions have emerged as the most employed models for explaining the observed suppression of $M_{2\nu}$ in addition to correlating the single-β GT strengths and half-lives of $2\nu\beta^-\beta^-$ decay by including a large number of basis states in the model space.

Many Body Approaches and Some Inferences

The necessity for the inclusion of nuclear deformation has resulted in the employment of deformed QRPA, projected-Hartree-Fock-Bogoliubov (PHFB), pseudo-SU(3), IBM, and energy density functional (EDF) approaches in the calculation of NTMEs.

Many Body Approaches and Some Inferences

The necessity for the inclusion of nuclear deformation has resulted in the employment of deformed QRPA, projected-Hartree-Fock-Bogoliubov (PHFB), pseudo-SU(3), IBM, and energy density functional (EDF) approaches in the calculation of NTMEs.

Additionally, there are many possibilities for the inclusion of the model dependent form factors for the finite size of nucleons (FNS), short-range correlations (SRC), and the value of axial vector current coupling constant g_A. Each model has a different truncation scheme for the unmanageable Hilbert space, and employs a variety of residual interactions, resulting in NTMEs $M(0\nu)$, which are of the same order of magnitude but not identical.

Many Body Approaches and Some Inferences

In the analysis of uncertainties in NTMEs for $0\nu\beta^-\beta^-$ decay, the spread between the available calculated results was translated into an average of all the available NTMEs, and the standard deviation was treated as the measure of the theoretical uncertainty. Bilenky and Grifols have suggested that the possible observation of $0\nu\beta\beta$ decay in several nuclei could be employed to check the calculated NTMEs in a model independent way by comparing the ratios of the NTMEs-squared with the ratios of observed half-lives $T^{0\nu}_{1/2}$.

Model specific theoretical uncertainties have been analyzed in the QRPA approach. Further, a few studies on uncertainties in NTMEs due to the SRC have also been preformed.

Many Body Approaches and Some Inferences

Recently we have studied the effects of pseudoscalar and weak magnetism terms on the Fermi, Gamow-Teller (GT), and tensorial NTMEs for the $0\nu\beta^-\beta^-$ decay of ^{94,96}Zr, ^{98,100}Mo, ^{104}Ru, ^{110}Pd, ^{128,130}Te, and ^{150}Nd isotopes in the light Majorana neutrino mass mechanism.

Many Body Approaches and Some Inferences

Recently we have studied the effects of pseudoscalar and weak magnetism terms on the Fermi, Gamow-Teller (GT), and tensorial NTMEs for the $0\nu\beta^-\beta^-$ decay of ^{94,96}Zr, ^{98,100}Mo, ^{104}Ru, ^{110}Pd, ^{128,130}Te, and ^{150}Nd isotopes in the light Majorana neutrino mass mechanism.

In addition, we investigate effects due to deformation, FNS, and the SRC vis-a-vis the radial evolution of NTMEs. Uncertainties in NTMEs are calculated statistically by employing four different parameterizations of effective two-body interaction, form factors with two different parameterizations, and three different parameterizations of the SRC.
In the same theoretical formalism, the $0\nu\beta^-\beta^-$ decay involving classical Majorons and sterile neutrinos is also studied.

Many Body Approaches and Some Inferences

The detailed theoretical formalism required for the study of $0\nu\ \beta^-\beta^-$ decay due to the exchange of light Majorana neutrinos has been given by Simkovic et al. as well as Vergados. The observability of Majoron accompanied $0\nu\ \beta^-\beta^-$ decay in nine Majoron models has already been discussed by Hirsch et al and for the mechanism involving sterile neutrinos has been given by Benes et al.

Table of Contents

Nuclear Models I

Five different many-body approximate methods have been applied for the calculation of the $0\nu\beta\beta$-decay NME. These models can be broadly classified into three categories :

- Nuclear Shell Model and its variants
- Self-consistent Mean Field Models
  1. Quasiparticle Random Phase Approximation (QRPA) and its extensions
  2. Projected Hartree-Fock-Bogoliubov (PHFB) method
  3. Deformed Hartree-Fock (DHF) method
  4. Energy Density Functional (EDF) Method
- Alternative Models
  1. Interacting Boson Model (IBM)
  2. Single state dominance hypothesis (SSDH)
  3. Operator expansion method (OEM)
  4. Group theoretical models - SU(2), p-SU(3), SU(4), SO(5)

  ....

Nuclear Models II

The Nuclear Shell Model (NSM)

1. The NSM allows to consider only a limited number of orbits close to the Fermi level
2. but all possible correlations within the space are included.
3. Proton-proton, neutron-neutron and proton-neutron (isovector and isoscalar) pairing correlations in the valence space are treated exactly.
4. Proton and neutron numbers are conserved and angular momentum conservation is preserved.
5. The effective interactions are usually constructed starting from monopole corrected G matrices

Nuclear Models III

Quasiparticle Random Phase Approximation (QRPA)

1. The QRPA has the advantage of large valence space but is not able to comprise all the possible configurations.
2. the large model space guarantees that the Ikeda sum rule is fulfilled. This is crucial to describe correctly the Gamow-Teller strength.
3. The proton-proton and neutron-neutron pairings are considered. They are treated in the BCS approximation. Thus, proton and neutron numbers are not exactly conserved.
4. The many-body correlations are treated at the RPA level within the quasiboson approximation.
5. Two-body G-matrix elements, derived from realistic one-boson exchange potentials within the Brueckner theory, are used for the determination of nuclear wave functions.

Nuclear Models IV

The Projected Hartree-Fock-Bogoliubov Method (PHFB)

1. In the PHFB wave functions of good particle number and angular momentum are obtained by projection on the axially symmetric intrinsic HFB states.
2. In applications to the calculation of the $0\nu\beta\beta$-decay NMEs the nuclear Hamiltonian was restricted only to quadrupole interaction.
3. With a real Bogoliubov transformation without parity mixing one can describe only neutron pairs with even angular momentum and positive parity.

Nuclear Models V

The Deformed Hartree-Fock Model (DHF)

Convenient choice in the higher mass region:

1. Difficult to perform the Shell model calculation in this region
2. Possibility of getting the shell model calculation in DHF by mixing a few intrinsic states

   Macfarlane & Shukla PLB 35, 11 (1971), Khadkikar et. al., PLB 36, 290 (1971), D. Ahalpara, JPG 11, 735 (1985)
3. Pairing is accounted by considering pair wise occupations of the HF single particle orbits (time-like and time-reversed) of the nuclei. Furthermore, the additional pairing effects are included by K=0 type particle-hole excitations (2p-2h, 4p-4h etc.) across the Fermi surfaces.
4. DHF has been successful in predicting the back-bending, band structure, B(E2) transition probabilities, signature effects and high K isomerism.

Nuclear Models VI

The Energy Density Functional Method (EDF)

1. The EDF is considered to be an improvement with respect to the PHFB.
2. The density functional methods based on the Gogny functional are taken into account.
3. The particle number and angular momentum projection for parent and daughter nuclei is performed and configuration mixing within the generating coordinate method is included.
4. A large single particle basis (11 major oscillator shells) is considered. Results are obtained for all nuclei of experimental interest.

Nuclear Models VII

Interacting Boson Model (IBM)

1. In the IBM the low lying states of the nucleus are modeled in terms of bosons. The bosons are in either L=0 (s boson) or L=2 (d boson) states.
2. one is restricted to 0^+ and 2^+ neutron pairs transferring into two protons.
3. The bosons interact through one- and two-body forces giving rise to bosonic wave functions.

Nuclear Models VIII

The differences among the listed methods of NME calculations for the $0\nu\beta\beta$-decay are due to the following reasons:

1. The mean field is used in different ways. As a result, single particle occupancies of individual orbits of various methods differ significantly from each other
2. The residual interactions are of various origin and renormalized in different ways.
3. Various sizes of the model space are taken into account.
4. Different many-body approximations are used in the diagonalization of the nuclear Hamiltonian.

Nuclear Models IX

Each of the applied methods has some advantages and drawbacks.

- The advantage of the ISM calculations is their full treatment of the nuclear correlations, which tends to diminish the NMEs.
- On the contrary, the QRPA, the EDF, and the IBM underestimate the multipole correlations in different ways and tend to overestimate the NMEs.
- The drawback of the ISM the limited number of orbits in the valence space and as a consequence the violation of Ikeda sum rule and underestimation of the NMEs.

The closure approximation

The $0\nu\beta\beta$-decay matrix elements are usually calculated using the closure approximation for intermediate nuclear states. Within this approximation energies of intermediate states $(E_n - E_i)$ are replaced by an average value $\overline{E} \approx 10$ MeV, and the sum over intermediate states is taken by closure, $\sum_n |n><n| = 1$. This simplifies the numerical calculation drastically. It was found that the differences in nuclear matrix elements are within 10%. The the dependence of the NMEs on the average energy of the intermediate states $\overline{E}$ was studied within the nuclear shell model. By varying $\overline{E}$ from 2.5 to 12.5 MeV the variation in the NME was obtained to be less than 5%

Table of Contents

Band Spectra

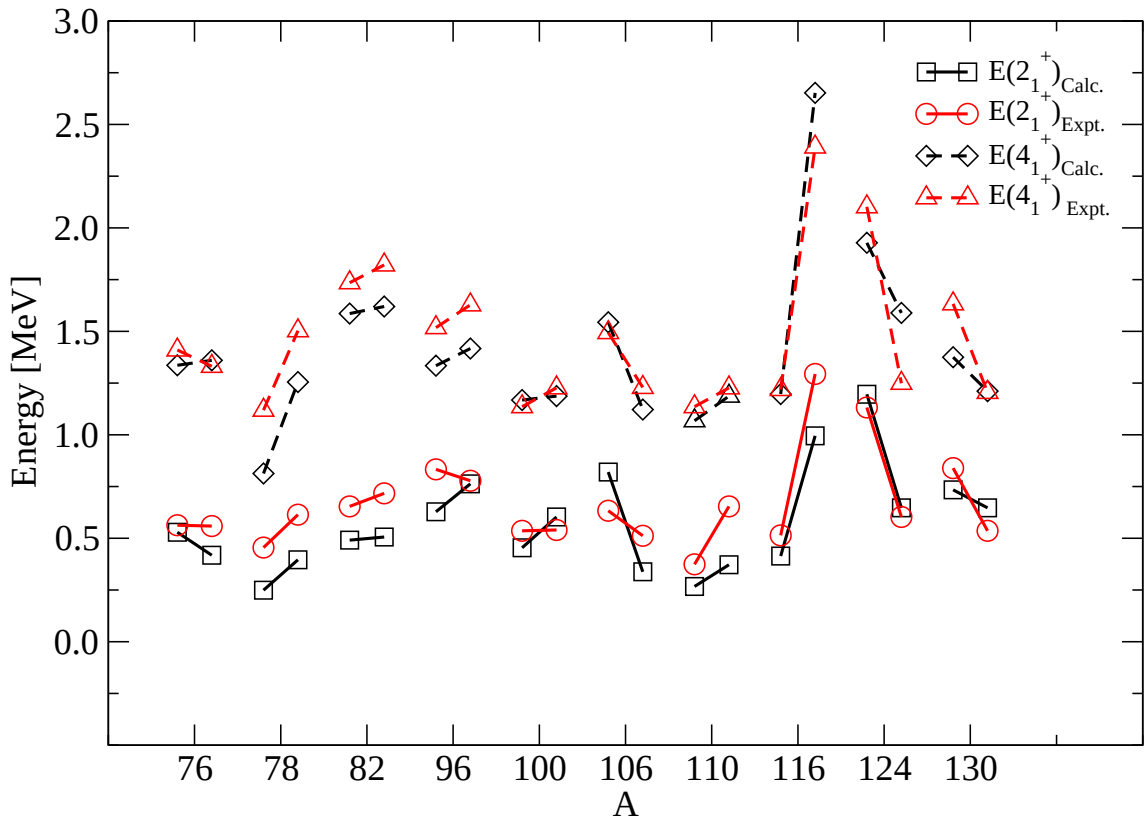

Figure: Comparision of calculated and experimental 2_1^+ and 4_1^+ energies .

Band Spectra : Even-Even nuclei

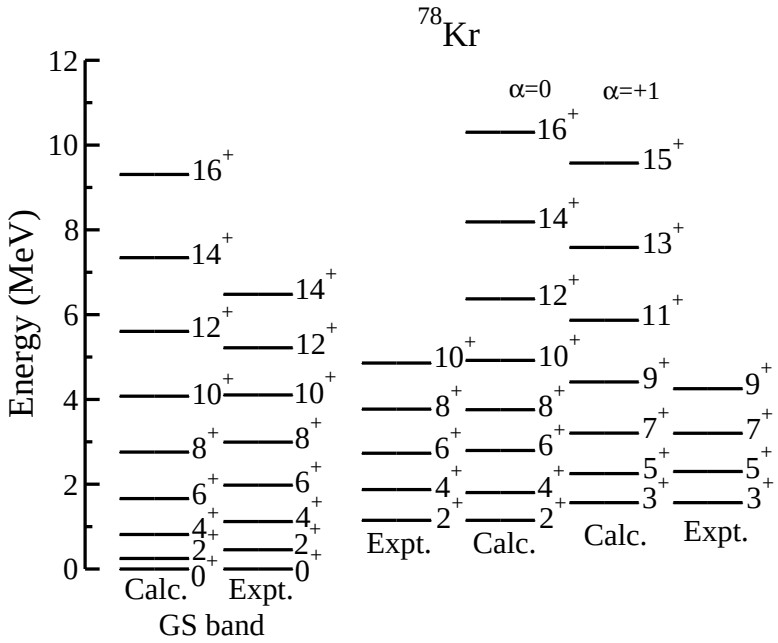

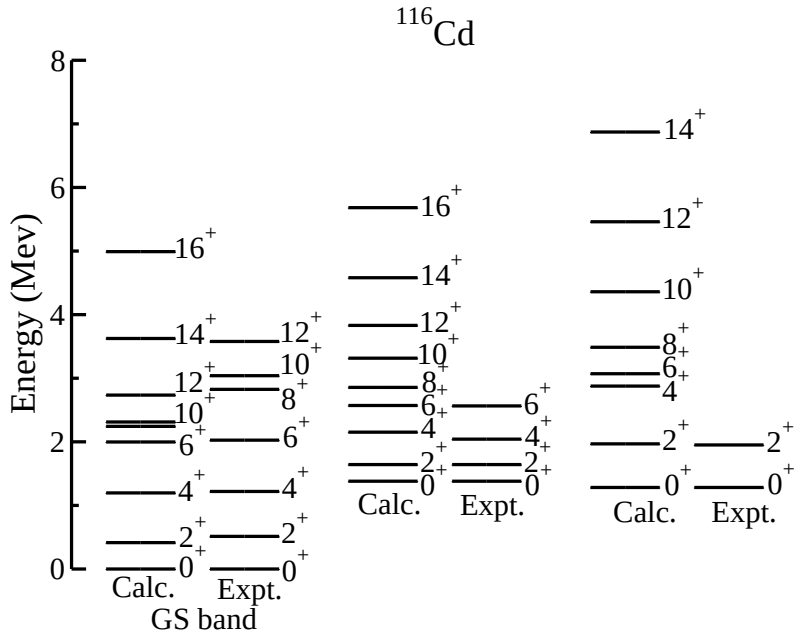

Band Spectra : Odd-Odd Nuclei

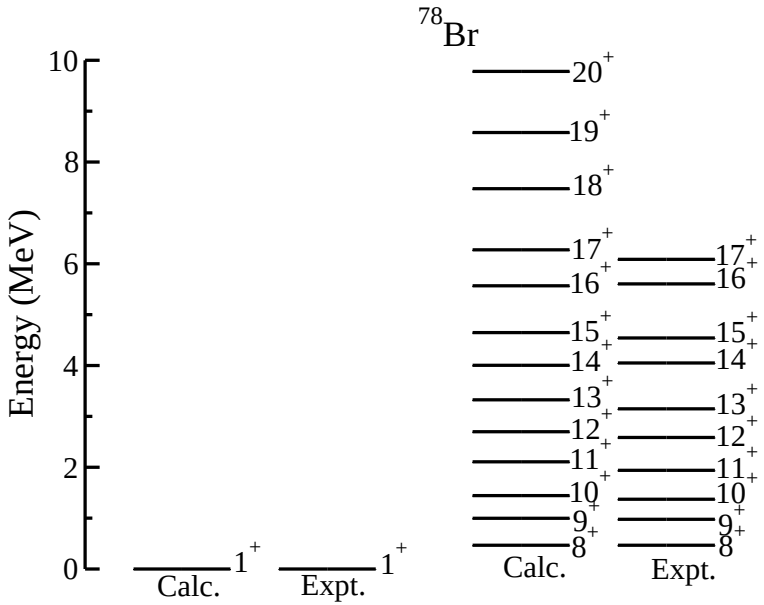

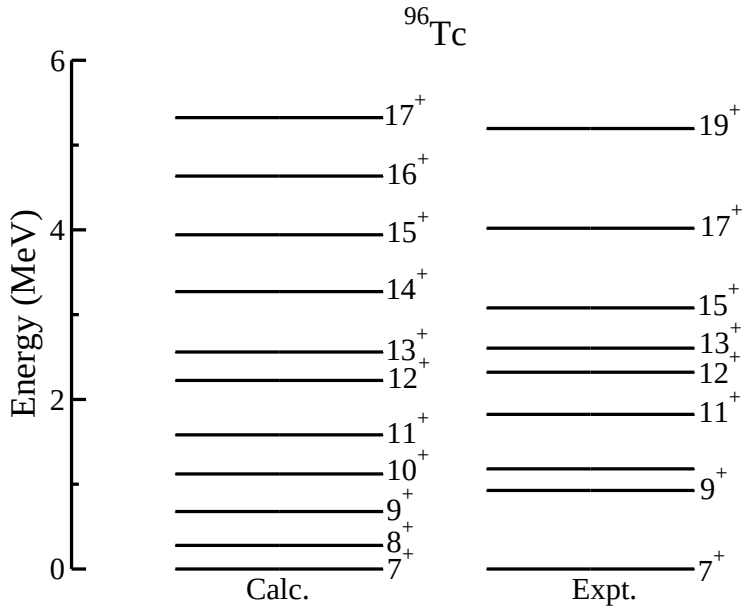

B(E2)

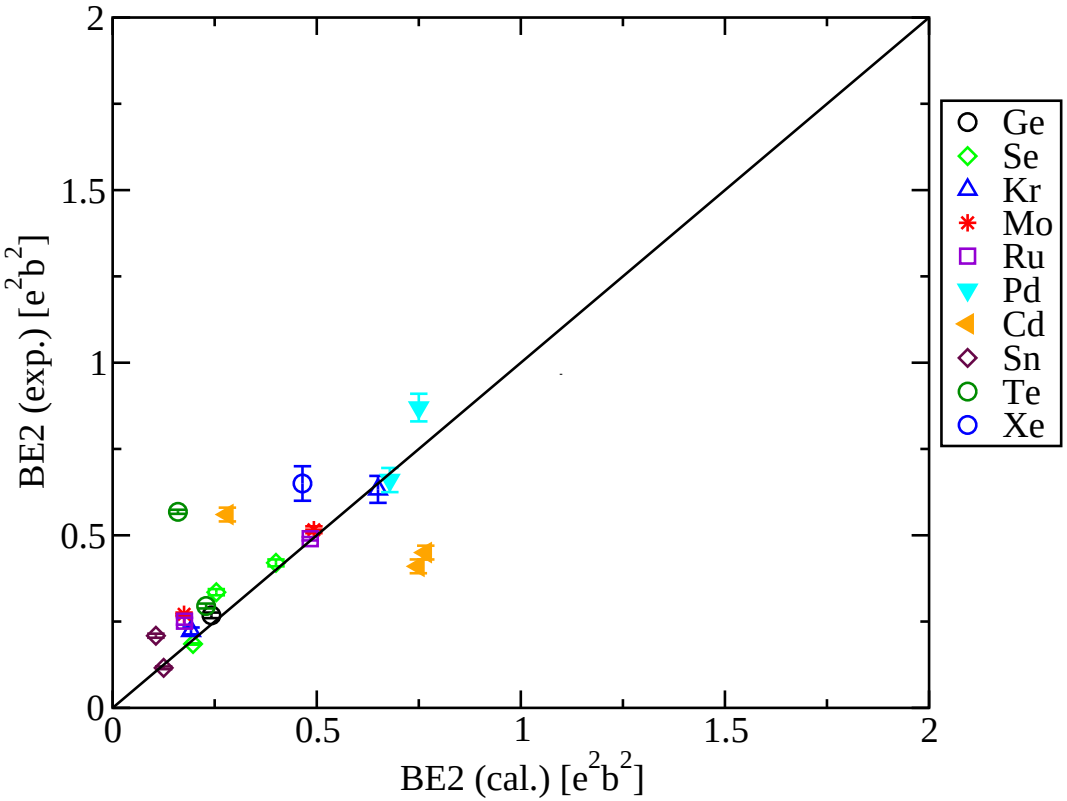

Figure: Comparison of calculated and experimental B(E2) values.

Quadrupole Moments

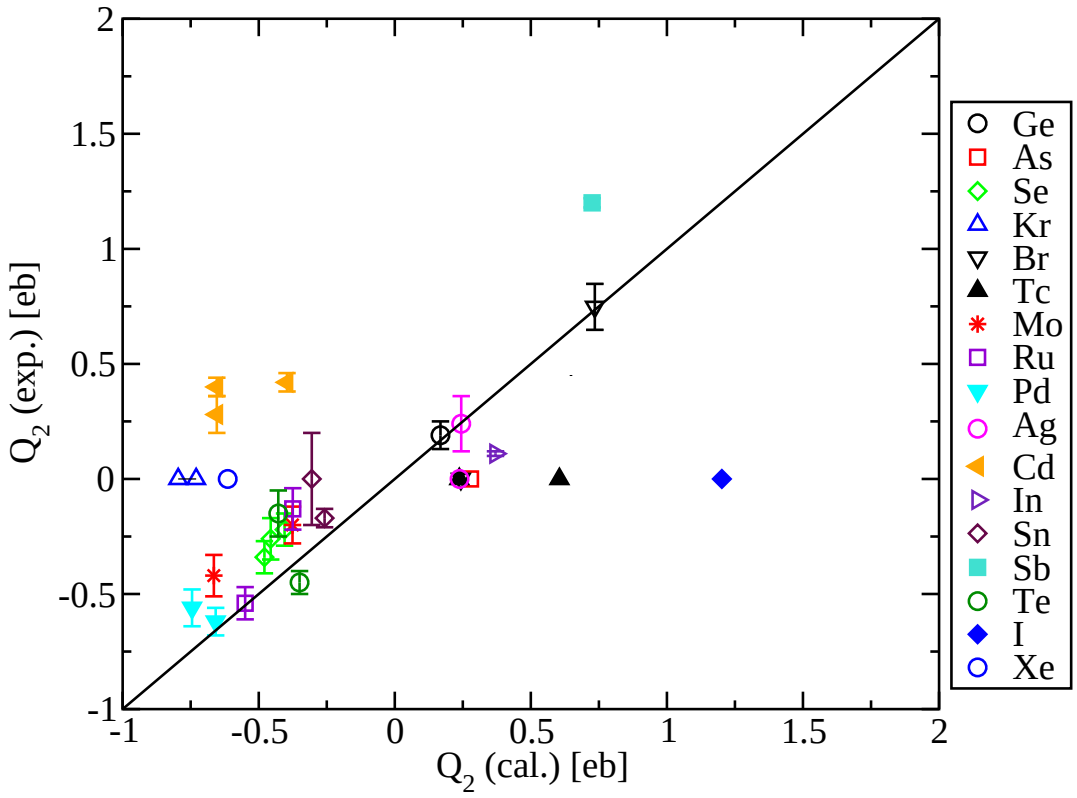

Figure: Comparision of calculated and experimental quadrupole moments.

Magnetic Moments

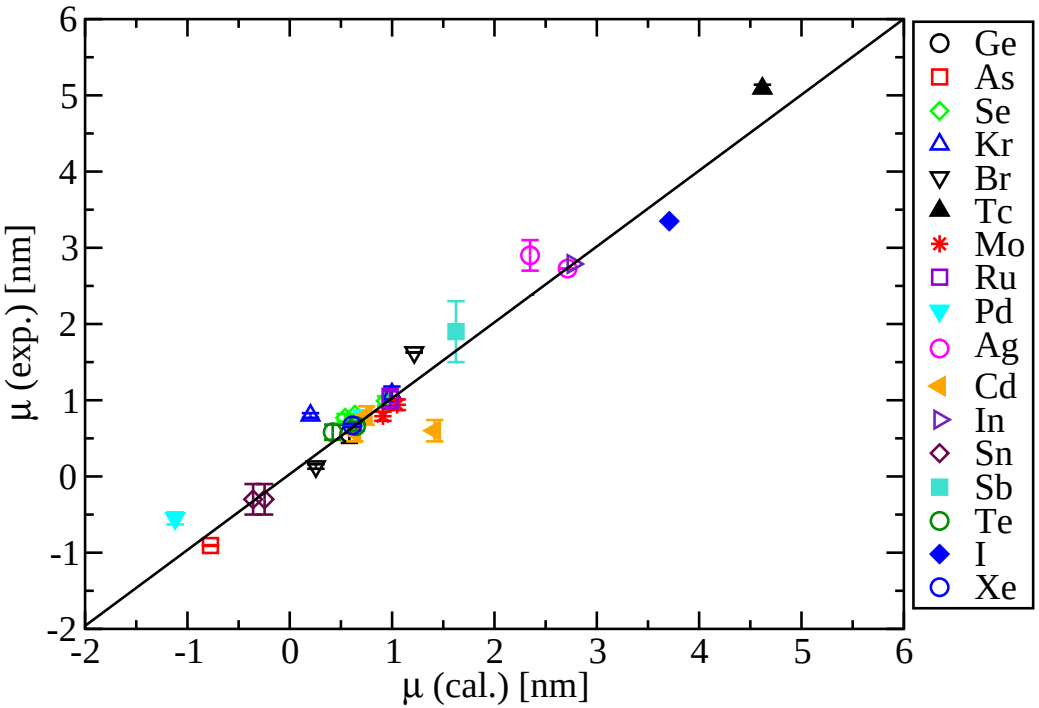

Figure: Comparison of calculated and experimental magnetic dipole moments for various nuclei.

The quenching of spin g-factors by 0.75 is used

Nuclear Transition Matrix Elements

The nuclear $\beta\beta$ decay is a second order process in weak interaction. The inverse half-life of the 2ν $\beta\beta$ decay for the $0^+ \rightarrow 0^+$ transition can be written as

$$[T^{2\nu}_{1/2}(0^+ \rightarrow 0^+)]^{-1} = G_{2\nu} \left| M_{2\nu} \right|^2$$

where $G_{2\nu}$ is the integrated kinematical factor and can be calculated with good accuracy. The nuclear transition matrix element (NTME) $M_{2\nu}$, which is a model dependent quantity, is given by

$$M_{2\nu} = \sum_N \frac{\langle 0^+ || \sigma\tau^{\pm} || 1^+_N \rangle \langle 1^+_N || \sigma\tau^{\pm} || 0^+ \rangle}{E_N - (E_I + E_F)/2}$$

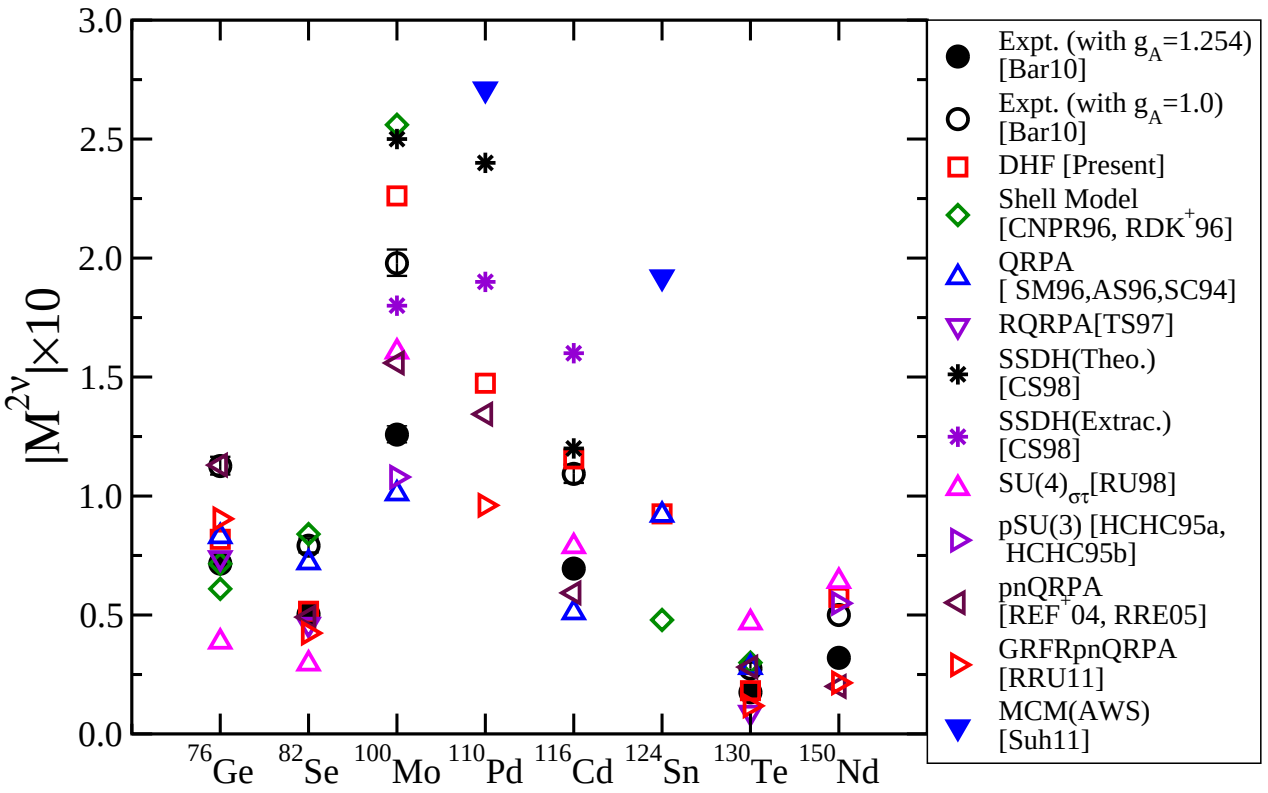

Figure: Comparison of calculated NTMEs with available experimental results for $2\nu\ \beta^-\beta^-$ decay of ^{76}Ge, ^{82}Se, ^{100}Mo, ^{110}Pd, ^{116}Cd, ^{124}Sn, ^{130}Te and ^{150}Nd isotopes for the $0^+(\text{gs}) \rightarrow 0^+(\text{gs})$ transition.

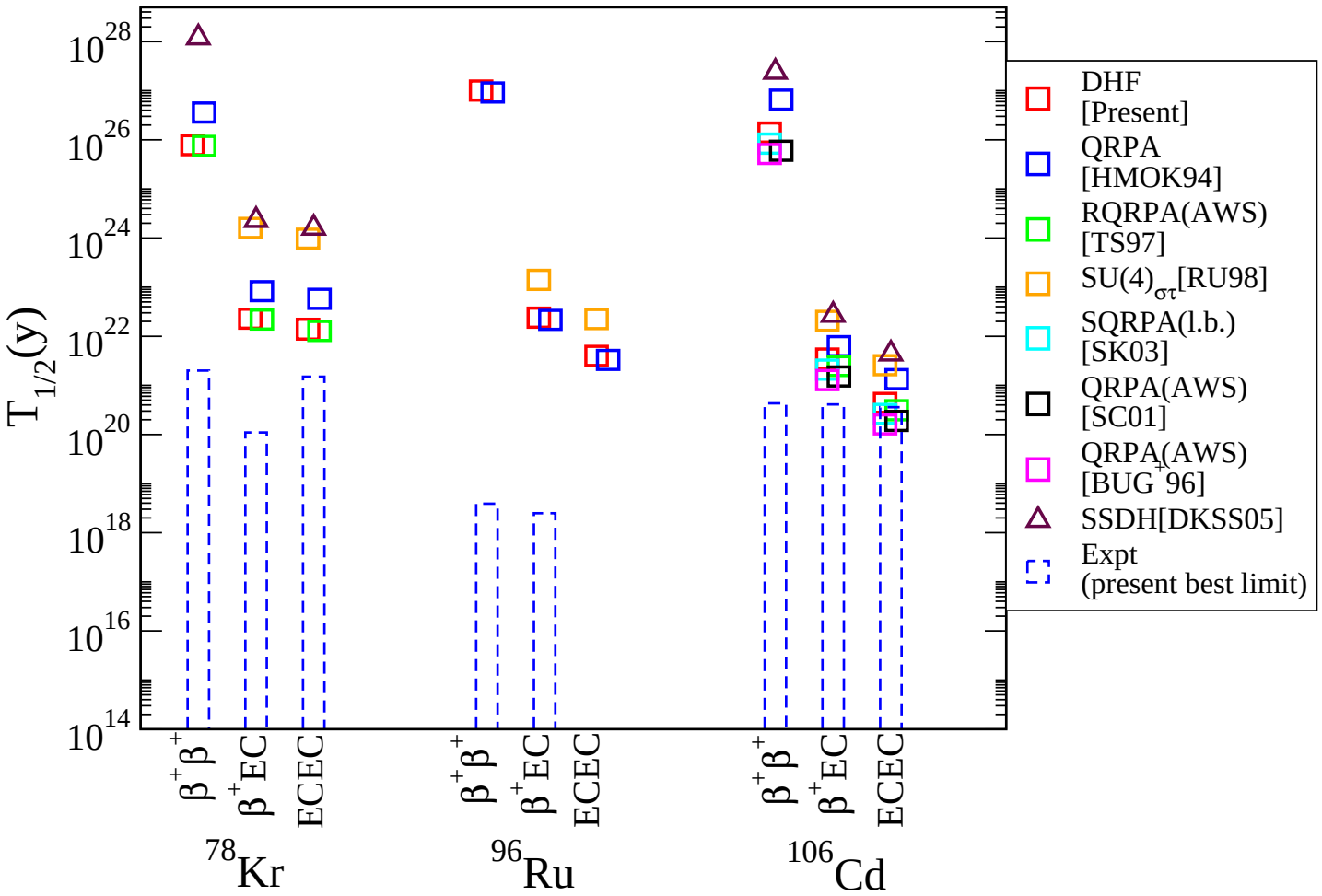

Figure: Comparison of predicted half-lives with the best available experimental limits for 2ν $\beta^+\beta^+$ / β^+EC/ ECEC decay of ^{78}Kr, ^{96}Ru and ^{106}Cd isotopes for the $0^+(\text{gs}) \rightarrow 0^+(\text{gs})$ transition.

Table of Contents

Light Majorona neutrino mass mechanism I

In the Majorana neutrino mass mechanism, the half-life $T_{1/2}^{(0\nu)}$ for the $0^+ \rightarrow 0^+$ transition of $(\beta^-\beta^-)_{0\nu}$ decay due to the exchange of light Majorana neutrinos between nucleons having finite size is given by

$$\left[T_{1/2}^{(0\nu)}(0^+ \rightarrow 0^+)\right]^{-1} = G_{01}\left|\frac{\langle m_\nu \rangle}{m_e} M^{(0\nu)}\right|^2$$

where

$$\langle m_\nu \rangle = \sum_i{}' U_{ei}^2 m_i, \qquad m_i < 10 \ eV$$

The Phase-space factor is given by

$$G_{01} = \left[\frac{2\left(G_F \ g_A\right)^4 m_e^9}{64\pi^5 \ \left(m_e R\right)^2 \ln\left(2\right)}\right] \int_1^{T+1} F_0\left(Z_f, \varepsilon_1\right) F_0\left(Z_f, \varepsilon_2\right) p_1 \ p_2 \ \varepsilon_1 \varepsilon_2 \ d\varepsilon_1$$

In the closure approximation, the NTME $M^{(0\nu)}$ is defined as

Light Majorona neutrino mass mechanism II

$$M^{(0\nu)} = \sum_{n,m} \left\langle 0_F^+ \left\| \left[-\frac{H_F(r_{nm})}{g_A^2} + \sigma_n \cdot \sigma_m H_{GT}(r_{nm}) + S_{nm} H_T(r_{nm}) \right] \tau_n^+ \tau_m^+ \right\| 0_I^+ \right\rangle$$

with

$$S_{nm} = 3\left(\sigma_n \cdot \hat{\mathbf{r}}_{nm}\right)\left(\sigma_m \cdot \hat{\mathbf{r}}_{nm}\right) - \sigma_n \cdot \sigma_m$$

The neutrino potentials associated with Fermi, Gamow-Teller (GT) and tensor operators are given by

$$H_\alpha(r_{nm}) = \frac{2R}{\pi} \int \frac{f_\alpha\left(q r_{nm}\right)}{\left(q + \overline{A}\right)} h_\alpha(q) q dq$$

where $f_\alpha\left(q r_{nm}\right) = j_0\left(q r_{nm}\right)$ and $f_\alpha\left(q r_{nm}\right) = j_2\left(q r_{nm}\right)$ for $\alpha =$Fermi$/GT$ and tensor potentials, respectively.

FNS & SRC I

The effects due to the FNS are incorporated through the dipole form factors and the form factor related functions $h_F(q)$, $h_{GT}(q)$ and $h_T(q)$ are written as

$$
\begin{aligned}
h_F(q) &= g_V^2\left(q^2\right) \\
h_{GT}(q) &= \frac{g_A^2(q^2)}{g_A^2}\left[1-\frac{2}{3}\frac{g_P(q^2)q^2}{g_A(q^2)2M_p}+\frac{1}{3}\frac{g_P^2(q^2)q^4}{g_A^2(q^2)4M_P^2}\right]+\frac{2}{3}\frac{g_M^2(q^2)q^2}{g_A^2 4M_p^2} \\
&\approx \left(\frac{\Lambda_A^2}{q^2+\Lambda_A^2}\right)^4\left[1-\frac{2}{3}\frac{q^2}{(q^2+m_\pi^2)}+\frac{1}{3}\frac{q^4}{(q^2+m_\pi^2)^2}\right]+\left(\frac{g_V}{g_A}\right)^2\frac{\kappa^2 q^2}{6M_p^2}\left(\frac{\Lambda_V^2}{q^2+\Lambda_V^2}\right)^4 \\
h_T(q) &= \frac{g_A^2(q^2)}{g_A^2}\left[\frac{2}{3}\frac{g_P(q^2)q^2}{g_A(q^2)2M_p}-\frac{1}{3}\frac{g_P^2(q^2)q^4}{g_A^2(q^2)4M_P^2}\right]+\frac{1}{3}\frac{g_M^2(q^2)q^2}{g_A^2 4M_p^2} \\
&\approx \left(\frac{\Lambda_A^2}{q^2+\Lambda_A^2}\right)^4\left[\frac{2}{3}\frac{q^2}{(q^2+m_\pi^2)}-\frac{1}{3}\frac{q^4}{(q^2+m_\pi^2)^2}\right]+\left(\frac{g_V}{g_A}\right)^2\frac{\kappa^2 q^2}{12M_p^2}\left(\frac{\Lambda_V^2}{q^2+\Lambda_V^2}\right)^4
\end{aligned}
$$

where

$$g_V(q^2) = g_V \left(\frac{\Lambda_V^2}{q^2 + \Lambda_V^2} \right)^2$$

$$g_A(q^2) = g_A \left(\frac{\Lambda_A^2}{q^2 + \Lambda_A^2} \right)^2$$

$$g_P(q^2) = \frac{2M_p g_A(q^2)}{(q^2 + m_\pi^2)} \left(\frac{\Lambda_A^2 - m_\pi^2}{\Lambda_A^2} \right)$$

$$g_M(q^2) = \kappa g_V\left(q^2\right)$$

with $g_V = 1.0$, $g_A = 1.254$, $\kappa = \mu_p - \mu_n = 3.70$, $\Lambda_V = 0.850$ GeV and $\Lambda_A = 1.086$ GeV.

FNS & SRC III

Consideration of internal structure of protons and neutrons suggests an alternative parametrization of $g_V(q^2)$ given by

$$g_V(q^2) = F_1^p(q^2) - F_1^n(q^2)$$

where

$$F_1^p(q^2) = \frac{1}{\left(1+\frac{q2}{4M^2}\right)}\left(\frac{\Lambda_V^2}{q^2+\Lambda_V^2}\right)^2\left[1+(1+\mu_p)\frac{q2}{4M^2}\right]$$

$$F_1^n(q^2) = \frac{\mu_n}{\left(1+\frac{q2}{4M^2}\right)}\left(\frac{\Lambda_V^2}{q^2+\Lambda_V^2}\right)^2(1-\xi_n)\frac{q2}{4M^2}$$

with $\mu_p = 1.79$ nm, $\mu_n = -1.91$ nm and $\Lambda_V = 0.84$ GeV.
In addition,

$$g_M(q^2) = F_2^p(q^2) - F_2^n(q^2)$$

FNS & SRC IV

where

$$F_2^p(q^2) = \frac{\mu_p}{\left(1+\frac{q2}{4M^2}\right)}\left(\frac{\Lambda_V^2}{q^2+\Lambda_V^2}\right)^2$$

$$F_2^n(q^2) = \frac{\mu_n}{\left(1+\frac{q2}{4M^2}\right)}\left(\frac{\Lambda_V^2}{q^2+\Lambda_V^2}\right)^2\left(1+\frac{q2}{4M^2}\xi_n\right)$$

with

$$\xi_n = \frac{1}{1+\lambda_n\frac{q2}{4M^2}}$$

and $\lambda_n = 5.6$.

FNS & SRC V

Explicitly, the effects due to the SRC can be incorporated in the calculation of $M^{(0\nu)}$ through the prescription

$$O_k \rightarrow fO_k f$$

with

$$f(r) = 1 - ce^{-ar^2}(1 - br^2)$$

where $a = 1.1$, 1.59 and 1.52 fm^{-2}, $b = 0.68$, 1.45 and 1.88 fm^{-2} and $c = 1.0$, 0.92 and 0.46 for Miller-Spencer, Argonne V18 and CD-Bonn NN potentials, respectively.

FNS & SRC VI

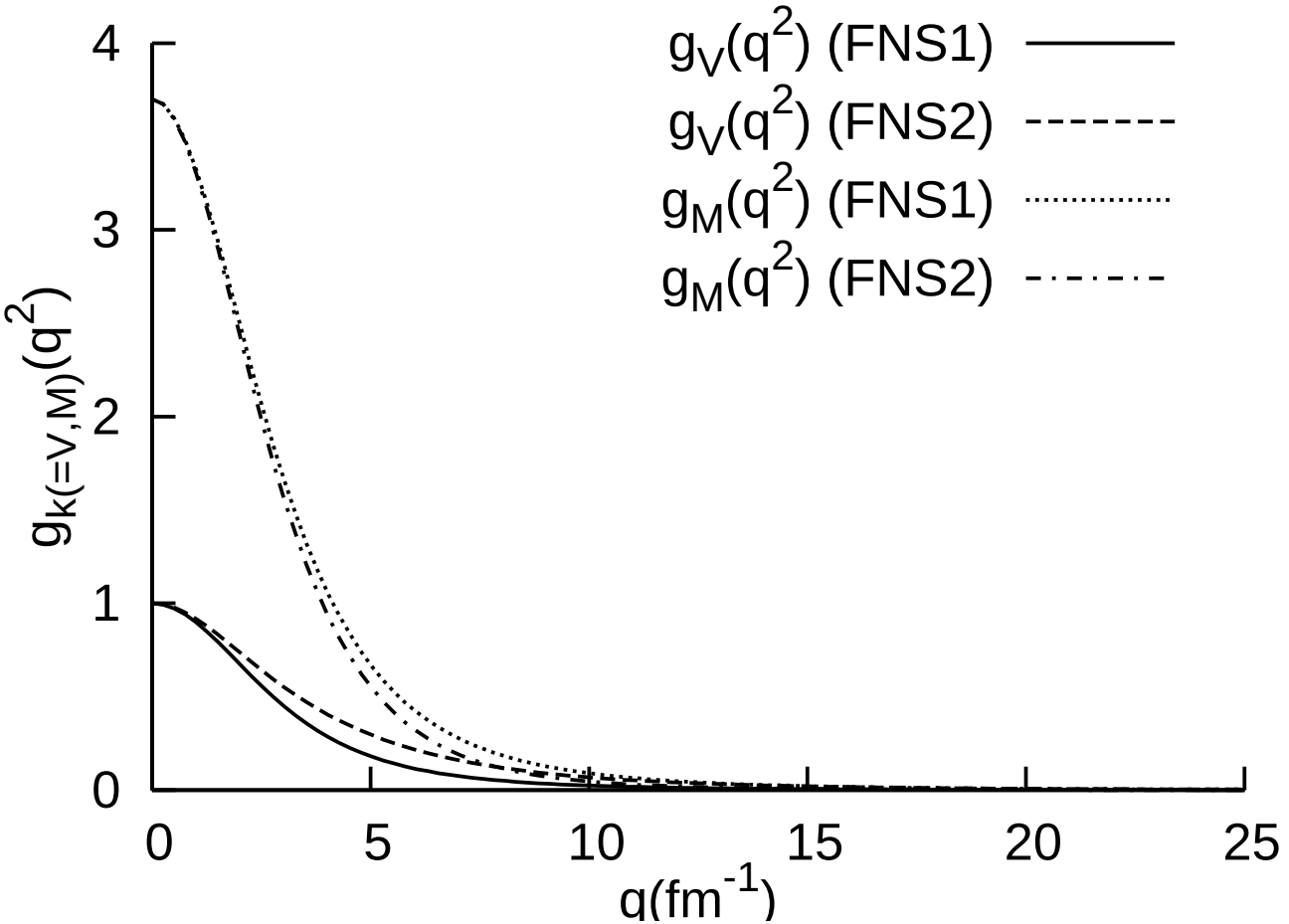

Figure: Distribution of $g_V(q^2)$ and $g_M(q^2)$ for FNS1 and FNS2.

Decomposition of NTMEs $M^{(0\nu)}$ for the $(\beta^-\beta^-)_{0\nu}$ decay of ^{100}Mo including higher order currents (HOC) with (a) FNS1, (b) FNS2 and SRC (HOC+SRC) for the $PQQ1$ parameterization.

NTMEs	FNS	HOC	HOC+SRC			HOC+SRC ($\bar{A}/2$)		
			SRC1	SRC2	SRC3	SRC1	SRC2	SRC3
$M_F^{(0\nu)}$	(a)	2.1484	1.8911	2.1492	2.2216	2.0691	2.3412	2.4168
	(b)	2.2034	1.9152	2.1883	2.2707	2.0943	2.3817	2.4673
$M_{GT-AA}^{(0\nu)}$		-6.3815	-5.4584	-6.3022	-6.5663	-5.9813	-6.8682	-7.1424
$M_{GT-PP}^{(0\nu)}$		-0.4503	-0.2962	-0.4054	-0.4510	-0.3060	-0.4177	-0.4640
$M_{GT-AP}^{(0\nu)}$		1.5521	1.1518	1.4644	1.5810	1.2013	1.5222	1.6413
$M_{GT-MM}^{(0\nu)}$	(a)	-0.2370	-0.1192	-0.1832	-0.2201	-0.1239	-0.1892	-0.2266
	(b)	-0.2311	-0.1222	-0.1850	-0.2187	-0.1269	-0.1909	-0.2251
$M_{GT}^{(0\nu)}$	(a)	-5.5167	-4.7220	-5.4265	-5.6564	-5.2098	-5.9529	-6.1918
	(b)	-5.5107	-4.7250	-5.4283	-5.6549	-5.2128	-5.9546	-6.1902
$M_{T-PP}^{(0\nu)}$		-0.0227	-0.0230	-0.0235	-0.0234	-0.0236	-0.0241	-0.0240
$M_{T-AP}^{(0\nu)}$		0.0692	0.0700	0.0710	0.0709	0.0718	0.0729	0.0728
$M_{T-MM}^{(0\nu)}$	(a)	0.0059	0.0060	0.0062	0.0062	0.0061	0.0064	0.0064
	(b)	0.0058	0.0058	0.0060	0.0060	0.0059	0.0062	0.0062
$M_T^{(0\nu)}$	(a)	0.0524	0.0529	0.0538	0.0537	0.0543	0.0552	0.0551
	(b)	0.0522	0.0528	0.0536	0.0535	0.0542	0.0550	0.0549
$\lvert M^{(0\nu)}\rvert$	(a)	6.8305	5.8716	6.7394	7.0155	6.4712	7.3865	7.6736
	(b)	6.8597	5.8902	6.7664	7.0454	6.4904	7.4142	7.7044

Radial Dependence

The radial evolution of $M^{(0\nu)}$ has been studied by defining

$$M^{(0\nu)} = \int C^{(0\nu)}(r)\, dr$$

Radial dependence of $C^{(0\nu)}(r)$ for the $(\beta^-\beta^-)_{0\nu}$ mode of ^{100}Mo isotope.

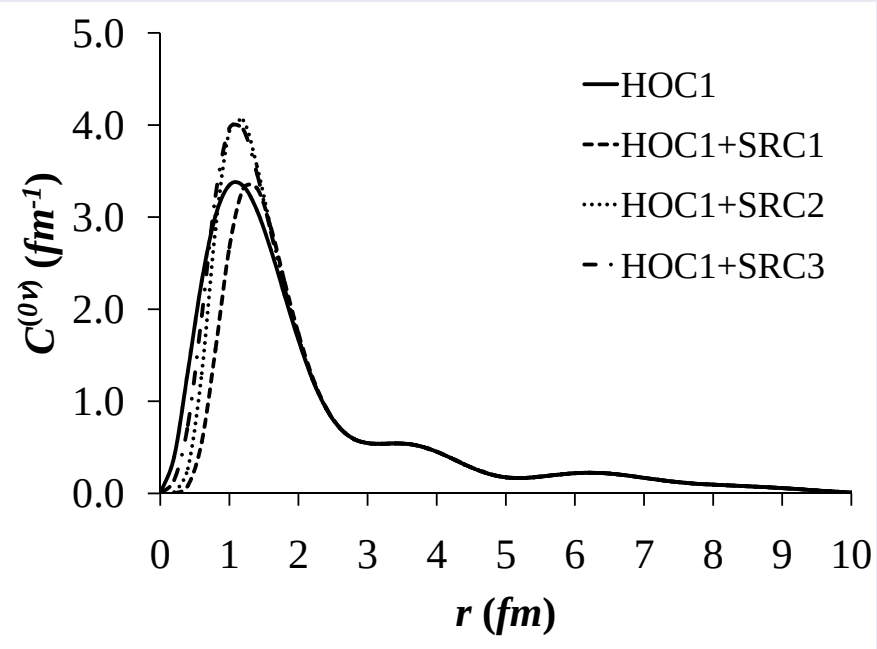

Radial Dependence

Radial dependence of $C^{(0\nu)}(r)$ for the $\left(\beta^-\beta^-\right)_{0\nu}$ mode of ^{96}Zr, ^{100}Mo, ^{110}Pd, ^{128,130}Te and ^{150}Nd isotopes. In this Fig., (a), (b), (c) and (d) correspond to HOC1, HOC1+SRC1, HOC1+SRC2 and HOC1+SRC3, respectively.

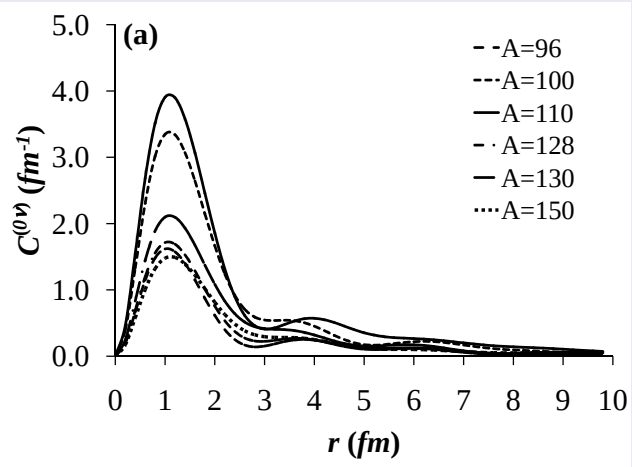

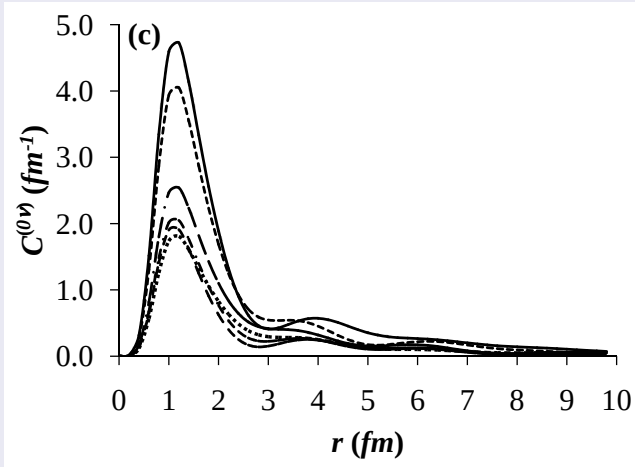

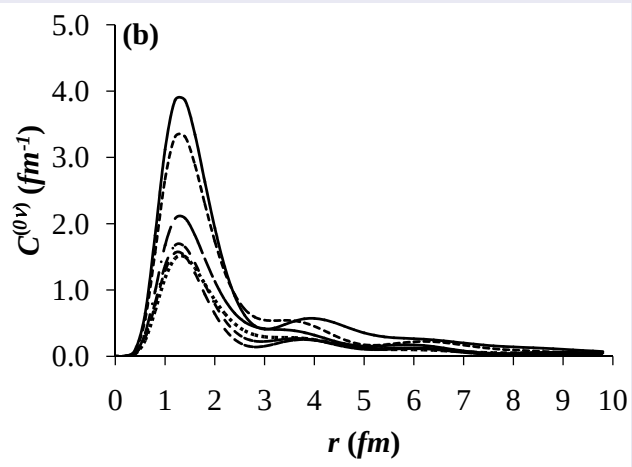

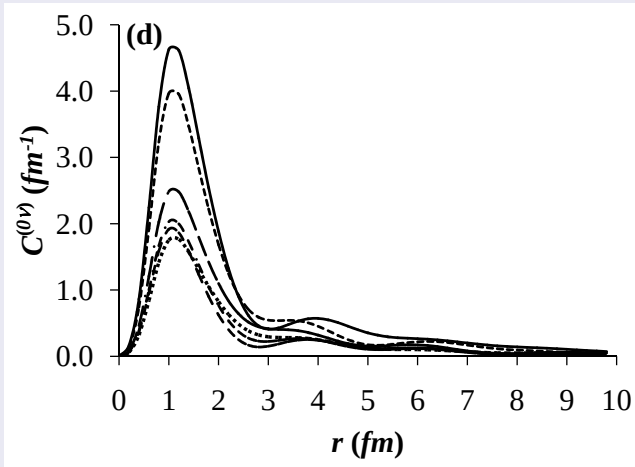

Effects due to FNS, HOC & SRC

Changes (in %) of the NTMEs $M^{(0\nu)}$ due to exchange of light Majorana neutrinos, for the $(\beta^-\beta^-)_{0\nu}$ decay with the inclusion of FNS1, HOC1 and HOC1+SRC (HOC1+SRC1, HOC1+SRC2 and HOC1+SRC3) for the four different parameterizations of the effective two-body interaction, namely (a) *PQQ*1, (b) *PQQHH*1, (c) *PQQ*2 and (d) *PQQHH*2.

	FNS1	HOC1		HOC1+SRC
(a)	8.94–10.63	11.17–12.96	(i)	12.38–15.61
			(ii)	0.99–1.96
			(iii)	2.48–2.97
(b)	9.40–11.07	11.43–13.03	(i)	13.17–16.40
			(ii)	1.11–2.11
			(iii)	2.50–3.04
(c)	8.95–10.68	10.13–13.00	(i)	12.40–15.71
			(ii)	0.99–1.99
			(iii)	2.39–2.99
(d)	9.25–11.15	11.38–12.73	(i)	12.91–16.56
			(ii)	1.07–2.15
			(iii)	2.51–3.06

Heavy Majorana Neutrinos

	FNS	F		F + S
(a)	26.53–29.72	15.26–18.00	(i)	65.46 – 68.22
			(ii)	40.13 – 42.37
			(iii)	18.35 – 19.61
(b)	26.75–29.97	15.29–17.13	(i)	65.72 – 67.91
			(ii)	40.33 – 42.17
			(iii)	18.46 – 19.52
(c)	26.53–29.76	13.62–17.99	(i)	64.57 – 68.25
			(ii)	39.60 – 42.39
			(iii)	18.10 – 19.63
(d)	26.66–30.03	15.31–17.08	(i)	65.74 – 68.04
			(ii)	40.34 – 42.27
			(iii)	18.46 – 19.58

Majoron accompanied $(\beta^-\beta^-)_{0\nu}$ decay I

In the classical Majoron model, the inverse half-life $T_{1/2}^{(0\nu\phi)}$ for the $0^+ \rightarrow 0^+$ transition of Majoron emitting $(\beta^-\beta^-\phi)_{0\nu}$ decay is given by

$$[T_{1/2}^{(0\nu\phi)}\left(0^+ \rightarrow 0^+\right)]^{-1} = |\langle g_M \rangle|^2 \, G_{0M} \left| M^{(0\nu\phi)} \right|^2$$

where $\langle g_M \rangle$ is the effective Majoron–neutrino coupling constant and the NTME $M^{(0\nu\phi)}$ is same as the $M^{(0\nu)}$ for the exchange of light Majorana neutrinos.

The phase space factors G_{0M} are evaluated by using

$$\begin{aligned} G_{0M} &= \left[\frac{2\left(G_F \; g_A\right)^4 m_e^9}{256\pi^7 \; \left(m_e R\right)^2 \ln\left(2\right)}\right] \int_1^{T+1} F_0\left(Z_f, \varepsilon_1\right) p_1 \; \varepsilon_1 \; d\varepsilon_1 \\ &\times \int_1^{T+2-\varepsilon_1} \left(T + 2 - \varepsilon_1 - \varepsilon_2\right) F_0\left(Z_f, \varepsilon_2\right) p_2 \; \varepsilon_2 d\varepsilon_2 \end{aligned}$$

Majoron accompanied $(\beta^-\beta^-)_{0\nu}$ decay II

Different Majoran models according to Bamert et al

Modes	Case	n	Pre-factor	Matrix elements
$\beta\beta\phi$	IB, IC, IIB	1	$\frac{2(G_F g_A)^4 m_e^9}{256\pi^7 ln(2)(m_e R)^2}$	$M_{CR}^{(0\phi)}$
$\beta\beta\phi$	IIC, IIF	3	$\frac{2(G_F g_A)^4 m_e^9}{64\pi^7 ln(2)(m_e R)^2}$	$M_{CR}^{(0\phi)}$
$\beta\beta\phi\phi$	ID, IE, IID	3	$\frac{2(G_F g_A)^4 m_e^9}{12288\pi^9 ln(2)(m_e R)^2}$	$M_{\omega^2}^{(0\phi)} = M_{F\omega^2} + M_{GT\omega^2}$
$\beta\beta\phi\phi$	IIE	7	$\frac{2(G_F g_A)^4 m_e^9}{215040\pi^9 ln(2)(m_e R)^2}$	$M_{\omega^2}^{(0\phi)} = M_{F\omega^2} + M_{GT\omega^2}$

Mechanism involving Sterile neutrinos I

The contribution of the sterile ν_h neutrino to the half-life $T_{1/2}^{(0\nu)}$ for the $0^+ \rightarrow 0^+$ transition of $(\beta^-\beta^-)_{0\nu}$ decay has been derived by considering the exchange of a Majorana neutrino between two nucleons and is given by

$$[T_{1/2}^{(0\nu)}(0^+ \rightarrow 0^+)]^{-1} = G_{01} \left| U_{eh}^2 \frac{m_h}{m_e} M^{0\nu}(m_h) \right|^2$$

U_{eh} is the $\nu_h - \nu_e$ mixing matrix element
The NTME $M^{0\nu}(m_h)$ is written as

$$M^{0\nu}(m_h) = \left\langle 0_F^+ \left\| \left[-\frac{H_F(m_h, r)}{g_A^2} + \sigma_n \cdot \sigma_m H_{GT}(m_h, r) + S_{nm} H_T(m_h, r) \right] \tau_n^+ \tau_m^+ \right\| 0_I^+ \right\rangle$$

The neutrino potentials are of the form

Mechanism involving Sterile neutrinos II

$$H_\alpha\left(m_h, r\right) = \frac{2R}{\pi}\int_0^\infty \frac{f_\alpha(qr)h_\alpha(q^2)q^2dq}{\sqrt{q^2+m_h^2}\left(\sqrt{q^2+m_h^2}+\overline{A}\right)}$$

Mechanism involving Sterile neutrinos III

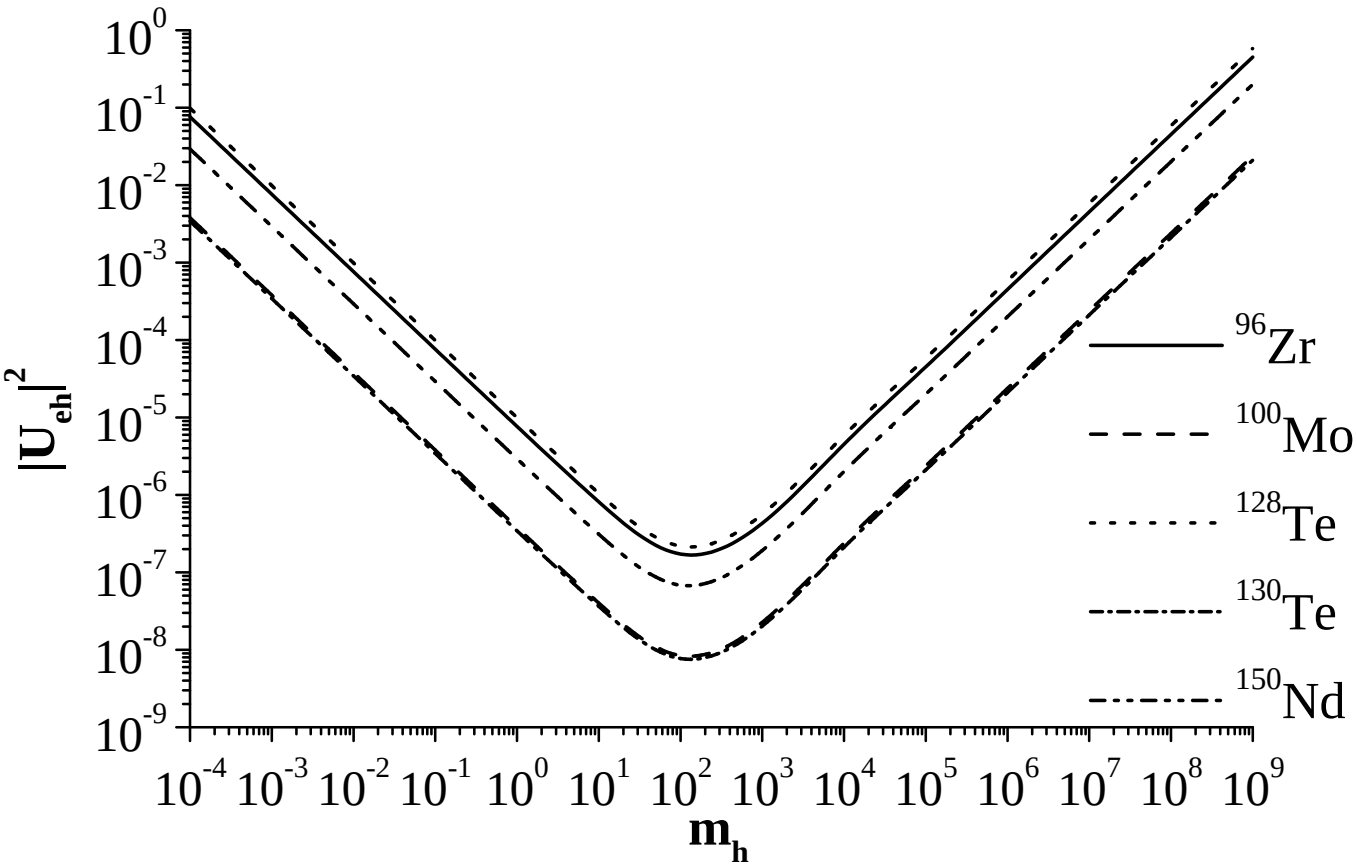

Figure: Variation in extracted limits on the $\nu_h - \nu_e$ mixing matrix element $|U_{eh}|^2$ with the mass m_h.

Deformation Effects

Deformation ratios $D^{(0\nu)}$ of $(\beta^-\beta^-)_{0\nu}$ decay for the $PQQ1$ parameterization.

Nuclei	HOC1	HOC1+SRC		
		SRC1	SRC2	SRC3
^{94}Zr	2.48	2.52	2.49	2.49
^{96}Zr	4.40	4.53	4.43	4.40
^{98}Mo	1.94	1.95	1.95	1.94
^{100}Mo	2.15	2.17	2.15	2.14
^{104}Ru	3.80	3.91	3.81	3.79
^{110}Pd	2.61	2.66	2.62	2.61
^{128}Te	4.38	4.50	4.40	4.38
^{130}Te	2.94	2.95	2.94	2.94
^{150}Nd	6.18	6.17	6.18	6.19

Deformation Effects

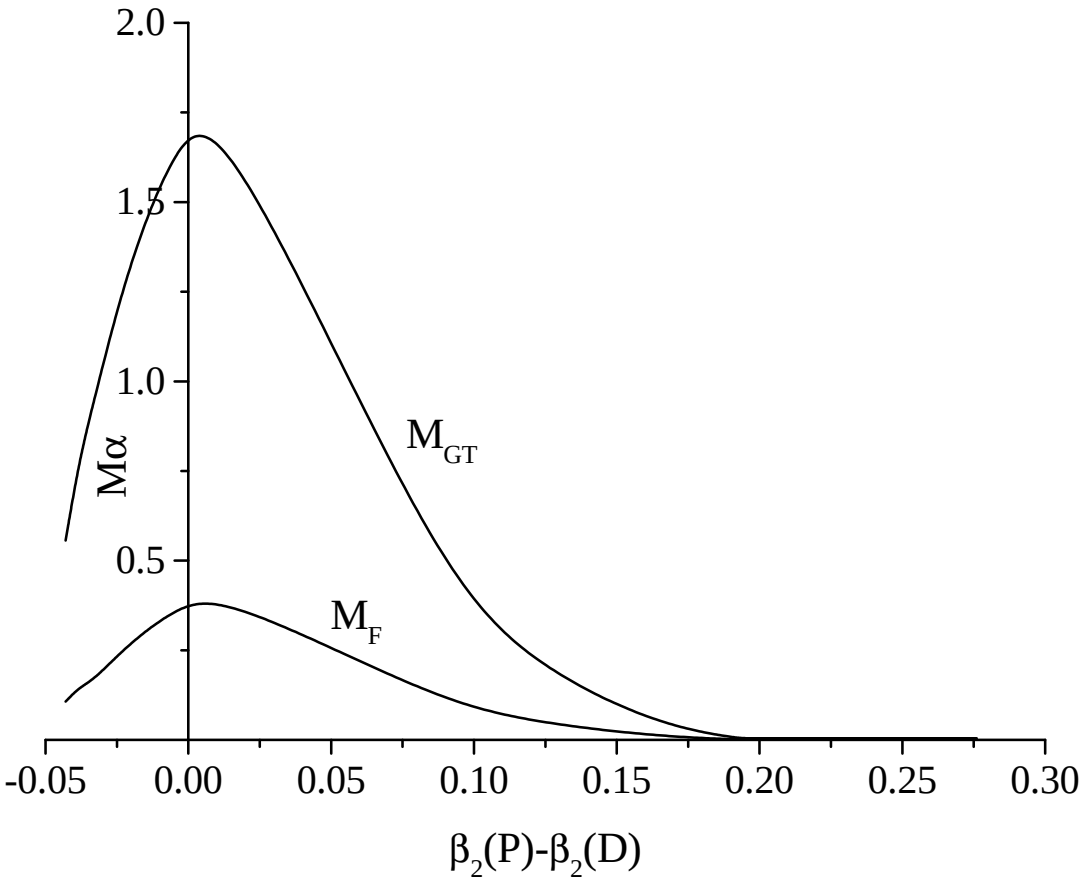

Figure: $0\nu\beta\beta$ NTME for ^{150}Nd as a function of the difference in the deformation parameter β_2 between the parent and daughte nuclei

Effect of QQ interaction

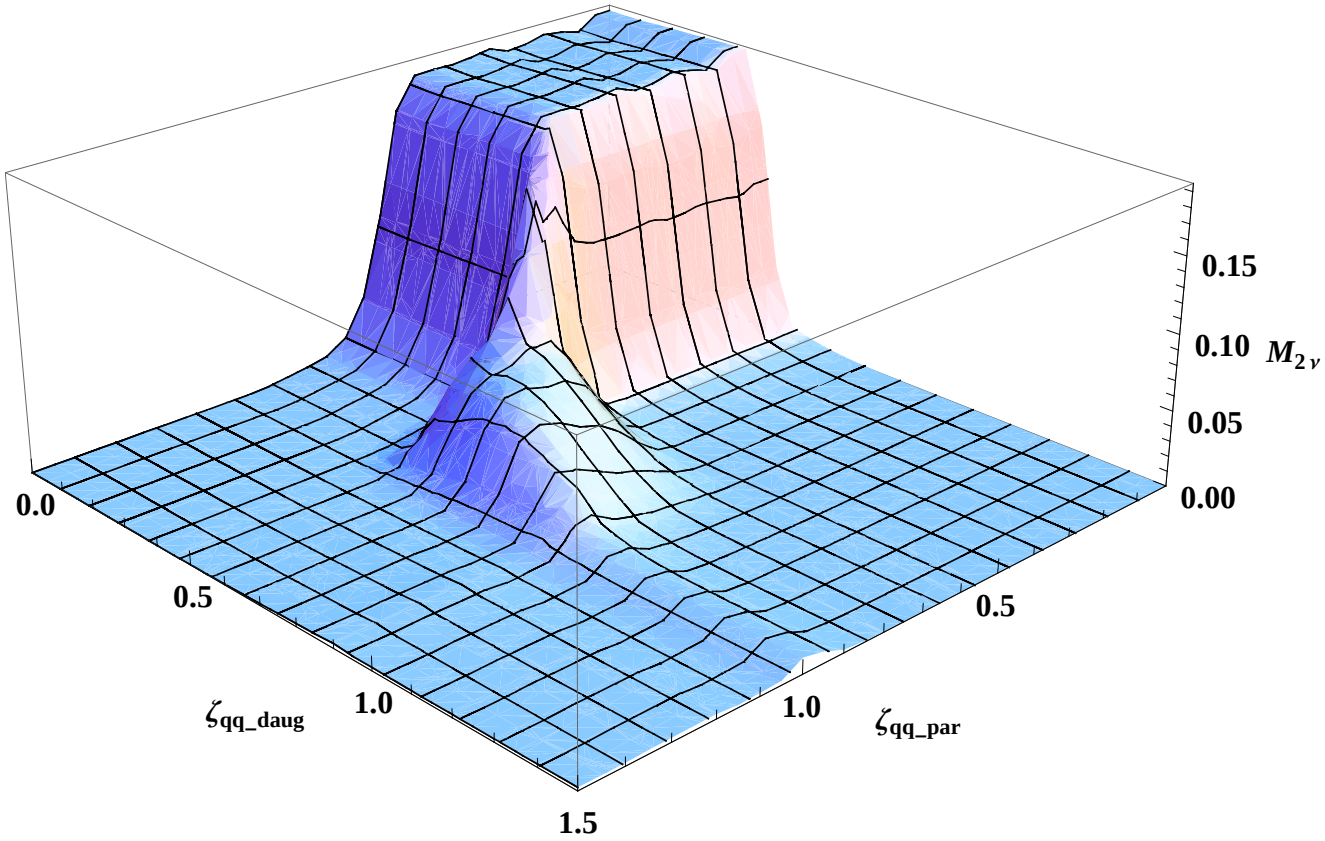

Figure: Dependence of $M_{2\nu}$ for ^{156}Dy on the independent variation of strength of QQ interaction ζ_{qq} for parent and daughter nuclei.

Deformation Effects

- NTMEs are large for a pair of spherical nuclei.
- With small admixture of quadrupolar correlations, NTMEs are almost constant and suppressed in realistic situations.
- NTMEs are large for identical deformations of parent and daughter nuclei.
- Sizes of NTMEs are reduced with the increase in deformations of parent and daughter nuclei.
- The deformation effects are equally important for $(\beta\beta)_{2\nu}$ and $(\beta\beta)_{0\nu}$ modes so far as nuclear structure aspect of $\beta\beta$ decay is concerned.

Table of Contents

Uncertainty of NTMEs

Average NTMEs $\overline{M}^{(0\nu)}$ and uncertainties $\Delta\overline{M}^{(0\nu)}$ for the $(\beta^-\beta^-)_{0\nu}$ decay of ^{94,96}Zr, ^{98,100}Mo, ^{110}Pd, ^{128,130}Te and ^{150}Nd isotopes(light Majorana Neutrino mass mechanism). Both bare and quenched values of g_A are considered.

$\beta^-\beta^-$ emitters	g_A	Case I		Case II	
		$\overline{M}^{(0\nu)}$	$\Delta\overline{M}^{(0\nu)}$	$\overline{M}^{(0\nu)}$	$\Delta\overline{M}^{(0\nu)}$
^{94}Zr	1.254	4.2464	0.3883	4.4542	0.2536
	1.0	4.6382	0.4246	4.8668	0.2759
^{96}Zr	1.254	3.1461	0.2778	3.3181	0.1243
	1.0	3.4481	0.3085	3.6376	0.1424
^{98}Mo	1.254	7.1294	0.6013	7.4656	0.3635
	1.0	7.8398	0.6826	8.2099	0.4358
^{100}Mo	1.254	6.8749	0.6855	7.2163	0.4977
	1.0	7.5660	0.7744	7.9419	0.5769
^{110}Pd	1.254	7.8413	0.8124	8.2273	0.6167
	1.0	8.6120	0.9184	9.0370	0.7128
^{128}Te	1.254	4.0094	0.4194	4.2175	0.3074
	1.0	4.4281	0.4601	4.6571	0.3355
^{130}Te	1.254	4.4458	0.5231	4.6633	0.4269
	1.0	4.9065	0.5837	5.1459	0.4802
^{150}Nd	1.254	3.1048	0.4649	3.2431	0.4434
	1.0	3.4334	0.5181	3.5856	0.4952

Uncertainty of NTMEs

Average NTMEs $\overline{M}_N^{(0\nu)}$ and uncertainties $\Delta\overline{M}_N^{(0\nu)}$ for the $(\beta^-\beta^-)_{0\nu}$ decay of ^{94,96}Zr, ^{98,100}Mo, ^{104}Ru, ^{110}Pd, ^{128,130}Te and ^{150}Nd isotopes (heavy Majorana Neutrino mass mechanism). Both bare and quenched values of g_A are considered. Case I and Case II denote calculations with and without SRC1, respectively.

$\beta^-\beta^-$	g_A	Case I		Case II	
emitters		$\overline{M}_N^{(0\nu)}$	$\Delta\overline{M}_N^{(0\nu)}$	$\overline{M}_N^{(0\nu)}$	$\Delta\overline{M}_N^{(0\nu)}$
^{94}Zr	1.254	126.2146	44.9489	152.8378	27.1912
	1.0	142.9381	49.1752	172.1620	29.3965
^{96}Zr	1.254	100.5313	36.8858	122.5048	21.9209
	1.0	114.4851	40.3246	138.6328	23.5263
^{98}Mo	1.254	202.5006	71.6345	245.3957	41.8882
	1.0	230.1520	78.3244	277.2795	44.9878
^{100}Mo	1.254	206.7533	73.0792	250.1870	43.7119
	1.0	235.0606	79.9885	282.7964	47.1334
^{104}Ru	1.254	150.5572	53.9389	182.7216	31.9382
	1.0	171.8075	59.0467	207.1750	34.3939
^{110}Pd	1.254	231.4743	82.4924	280.5688	49.1588
	1.0	263.4339	90.3033	317.3947	53.0150
^{128}Te	1.254	126.8285	46.3381	153.7370	29.4676
	1.0	143.9772	50.6942	173.5263	31.8554
^{130}Te	1.254	136.3856	46.9164	164.5378	27.2226
	1.0	154.3797	51.2511	185.2849	29.1907
^{150}Nd	1.254	85.5467	31.4473	103.4294	20.9802
	1.0	97.3640	34.5024	117.0160	22.8729

Uncertainty of NTMEs

Average NTMEs $\overline{M}^{(K)}$ and uncertainties $\Delta\overline{M}^{(K)}$ for $(\beta^+\beta^+)_{0\nu}$ and $(\varepsilon\beta^+)_{0\nu}$ modes of ^{96}Ru, ^{102}Pd, ^{106}Cd, ^{124}Xe, ^{130}Ba and ^{156}Dy isotopes. Both bare and quenched values of g_A are considered. Case I and Case II denote calculations with and without SRC1, respectively.

Nuclei	g_A	Light neutrino exchange				Heavy neutrino exchange			
		Case I		Case II		Case I		Case II	
		$\overline{M}^{(0\nu)}$	$\Delta\overline{M}^{(0\nu)}$	$\overline{M}^{(0\nu)}$	$\Delta\overline{M}^{(0\nu)}$	$\overline{M}^{(0N)}$	$\Delta\overline{M}^{(0N)}$	$\overline{M}^{(0N)}$	$\Delta\overline{M}^{(0N)}$
^{96}Ru	1.254	4.59	0.34	4.82	0.11	148.13	50.27	178.29	29.19
	1.0	5.13	0.40	5.39	0.13	165.91	59.74	201.49	35.61
^{102}Pd	1.254	4.71	0.60	4.97	0.50	160.83	58.13	195.01	35.86
	1.0	5.34	0.71	5.63	0.59	181.01	69.02	221.36	43.39
^{106}Cd	1.254	7.57	0.89	7.97	0.72	249.89	89.73	302.93	54.54
	1.0	8.52	1.04	8.98	0.84	281.22	106.57	343.82	66.13
^{124}Xe	1.254	3.50	0.42	3.69	0.32	124.84	44.75	151.45	26.71
	1.0	3.96	0.49	4.19	0.37	140.70	53.16	172.11	32.44
^{130}Ba	1.254	2.60	0.80	2.75	0.82	97.35	41.65	118.11	34.03
	1.0	2.94	0.90	3.12	0.92	109.75	48.71	134.24	39.56
^{156}Dy	1.254	2.22	0.31	2.33	0.29	72.96	26.36	87.78	18.02
	1.0	2.50	0.36	2.63	0.33	81.66	31.12	99.13	21.41

QRPA calculations of NTMEs

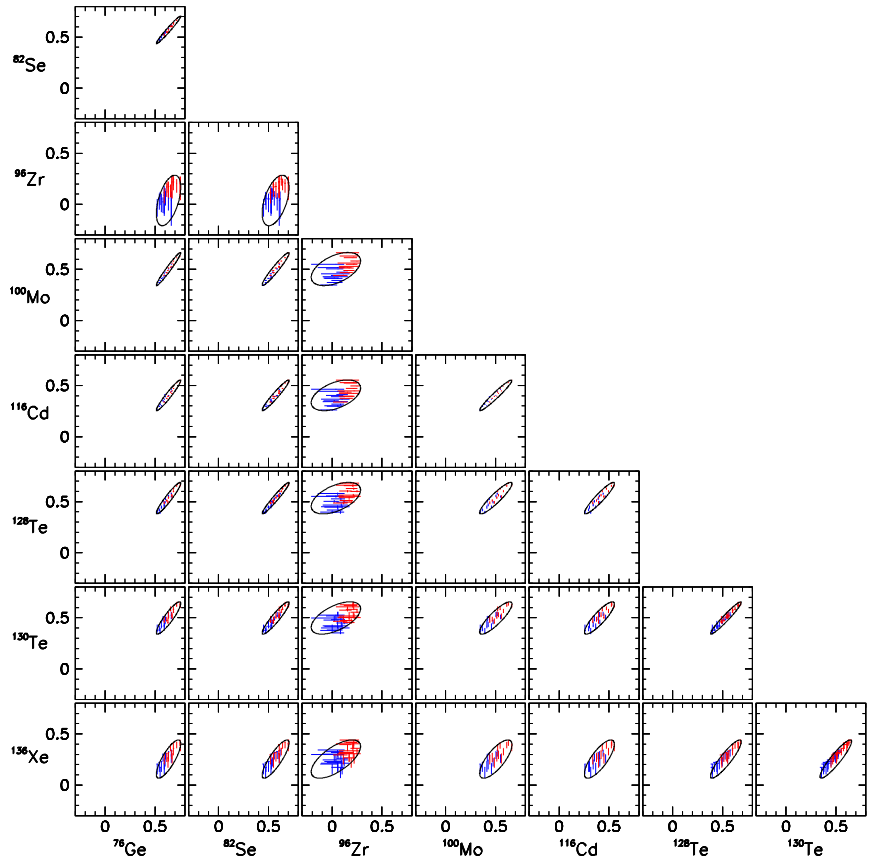

Figure: Scatter plot of estimated QRPA values for logarithms of the $0\nu\beta\beta$ matrix element for pairs of decaying nuclei, together with 1σ error ellipses. Error bars on points indicate uncertainty in the QRPA parameter gpp. Blue points are calculated with the MillerSpencer treatment of short-range correlation functions and red points with the UCOM treatment.

Taken from Phys. Rev. D 79 053001 (2009)

Table of Contents

Conclusions

Hadronizations (Structure of NTMEs)

Conclusions

Hadronizations (Structure of NTMEs)

Short range correlation and finite nuclear size

Conclusions

Hadronizations (Structure of NTMEs)

Short range correlation and finite nuclear size

Axial currents & Renormalization of g_A

Conclusions

- Hadronizations (Structure of NTMEs)
- Short range correlation and finite nuclear size
- Axial currents & Renormalization of g_A
- Calculation of NTMEs in different nuclear models

References I

1. Janet M. Conrad, William C. Louis, and Michael H. Shaevitz, Ann. Rev. of Nucl. and Part. Sci., Vol. 63, 45-67 (2013).
2. P. K. Rath et. al, EPJA 23, 223 (2005); EPJA 28, 27 (2006); EPJA 33, 375 (2007), PRC 78, 054302 (2008); PRC 80, 044303 (2009), EPL 86, 32001 (2009), JPG 37, 055108 (2010), PRC 88, 064322 (2013), PRC 87, 014301 (2013)
3. M Agostini (GERDA Collaboration), Phys. Rev. Lett. 111, 122503 (2013).
4. D. R. Artusa et al. (CUORE Collaboration), Eur. Phys. J. C 74, 2956 (2014).
5. M. Auger et. al. (EXO Collaboration), Phys. Rev. Lett. 109 (2012) 032505. E. Conti et al. Phys. Rev. B 68 (2003) 054201, hep-ex/0303008 preprint.
6. A. Gando A et al. (KamLAND-Zen Collaboration), Phys. Rev. C85 (2012) 045504.
7. A. S. Barabash (SuperNEMO Collaboration), J. Phys. Conf. Ser. 375 (2012) 042012.
8. D. G. Phillips II et al. (MAJORANA Collaboration),. J. Phys.: Conf. Ser. 381 (2012) 012044.
9. J. Maneira (SNO+ Collaboration), J. Phys.: Conf. Ser. 447, 012065 (2013).
10. I. Ogawa et al. (CANDLES) J. Phys. Conf. Ser. 375, 042018 (2012).
11. A. Giuliani (LUCIFER Collaboration), Acta Phys. Polon. B 41, 1447 (2010).
12. K. Zuber (COBRA Collaboration), Prog. Part. Nucl. Phys. 64, 267 (2010).
13. H. Bhang et al. (AMoRE) J. Phys. Conf. Ser. 375, 042023 (2012).

References II

14. H. Ejiri (MOON Collaboration), Nucl. Phys. A 844, 10c (2010).
15. V. Alvarez et al. (NEXT Collaboration), JINST 7, T06001 (2012) (Preprint arXiv:1202.0721).
16. A. Takeda (XMASS Collaboration), AIP Conf. Proc. 1338, 123 (2011).
17. T. Ishikawa et al. (DCBA Collaboration), Nucl. Instrum. Meth. A 628, 209 (2011).
18. M. Doi, T. Kotani and E. Takasugi, Prog. Theo. Phys. Suppl. 83, 1 (1985).
19. M. C. Gonzalez-Garcia and M. Maltoni, Phys. Rep., 460, 1 (2008).
20. S. M. Bilenky and C. Giunti, arXiv:1203.5250v3[hep-ph].
21. H. V. Klapdor-Kleingrothaus, A. Dietz, H. L. Harney, and I. V. Krivosheina, Mod. Phys. Lett. A 16, 2409 (2001); H. V. Klapdor-Kleingrothaus *et al.*, Eur. Phys. J. A 12, 147 (2001).
22. H. V. Klapdor-Kleingrothaus, I. V. Krivosheina, A. Dietz, and O. Chkvorets, Phys. Lett. B 586, 198 (2004).
23. F. Feruglio, A. Strumia and F. Vissani, Nucl. Phys. B 637, 345 (2002).
24. C. E. Aalseth *et al.*, Phys. Rev. D 65, 092007 (2002); Mod. Phys. Lett. A 17, 1475 (2002).
25. Yu. G. Zdesenko, F. A. Danevich, and V. I. Tretyak, Phys. Lett. B 546, 206 (2002).
26. A. Ianni, Nucl. Instrum. Meth. A 516, 184 (2004).

References III

27. G. L. Fogli, E. Lisi, A. Marrone, A. Palazzo, and A. M. Rotunno, Phys. Rev. D 84, 053007 (2011).
28. R. Arnold *et al.*, Phys. Rev. Lett. 107,062504 (2011); Nucl. Phys. A 765, 483 (2006); Nucl. Phys. A 678, 341 (2000).
29. A. Barabash and V. Brudanin (NEMO Collaboration), Phys. At. Nucl. 74, 312 (2011).
30. J. Argyriades *et al.*, Phys. Rev. C 80, 032501(R) (2009); Nucl. Phys. A 847, 168 (2010).
31. P. Bamert, C. P. Burgess and R. N. Mohapatra, Nucl. Phys. B 449, 25 (1995).
32. M. Hirsch, H. V. Klapdor-Kleingrothaus, S. G. Kovalenko, and H. Päs, Phys. Lett. B 372, 8 (1996).
33. C. Giunti and M. Laveder, Nucl. Phys. B Proc. Suppl. 217, 193 (2011).
34. F. Šimkovic, G. Pantis, J. D. Vergados, and A. Faessler, Phys. Rev. C 60, 055502 (1999).
35. J. D. Vergados, Phys. Rep. 361, 1 (2002).
36. E. Caurier, J. Menéndez, F. Nowacki, and A. Poves, Phys. Rev. Lett. 100, 052503 (2008).
37. J. Barea and F. Iachello, Phys. Rev. C 79, 044301 (2009).
38. F. Šimkovic, A. Faessler, H. Müther, V. Rodin, and M. Stauf, Phys. Rev. C 79, 055501 (2009).
39. J. Engel, J. Phys. G: Nucl. Part. Phys. 42, 034017 (2015).
40. A. Faessler, G. L. Fogli, E. Lisi, V. Rodin, A. M. Totunno and F. Šimkovic, Phys. Rev. C 79, 053001 (2009).
41. C. R. Praharaj, Physics Letters B 119, 17 (1982).
42. S. K. Ghorui, Ph. D. Thesis (unpublished), IIT Kharagpur (2012).

Collaborators

J. G. Hirsch
Instituto de Ciencias Nucleares
Universidad Nacional Autonona de Mexico

P. K. Rath
Department of Physics
University of Lucknow, India

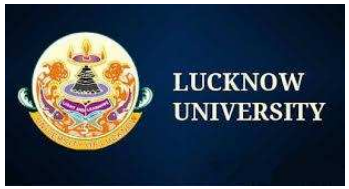

R. Chandra
Department of Applied Physics
BBA University, Lucknow, India

K. Chaturvedi
Department of Physics
Bundelkhand University, Jhansi, India

S. K. Ghorui
Department of Physics
Indian Institute of Technology Ropar, India

Thank You